INVESTIGATION OF Ag_2HgI_4 NANOPARTICLES: THERMAL PHASE TRANSITION AND NON-ISOTHERMAL KINETIC STUDY

A.M. MANSOUR[A*], I.M. EL RADAF[B], TALAAT A. HAMEED[A], G. B. SAKR[C]

Ag_2HgI_4 nano-powder was successively prepared by the solvothermal method. The structure and morphology of the resulted powder were characterized by X-ray diffraction technique, electron dispersive x-ray spectroscopy (EDX), and scanning electron microscope (SEM). Phase transformation was studied by differential thermal analysis (DTA) at 5, 10, 15, 20, 25, and 30 degrees/minute heating rates. The non-isothermal apparent activation energy of the attained thermal transitions was calculated by Kissinger, Flynn-Wall-Ozawa, and Augis-Bennett approaches respectively.

Keywords: Ag_2HgI_4; DTA; Kissinger; Flynn-Wall-Ozawa; Augis-Bennett

1. Introduction

A variety of solids exhibits transformations from one structure to one other by changing temperature [1]. The subject of phase transitions was increased extensively in last few years, with new types of transitions including new approaches to discuss the event. The high ionic conductivity achieved by many superionic conductors is through clear phase transitions, at particular temperatures [2–4]. During the phase transition, the free energy of the solid is kept constant but thermodynamic quantities including heat capacity, volume and entropy display discontinuous changes [5,6].

Phase transitions in solid are frequently associated with significant variations in its benefits. Several techniques are employed to inspect phase transition, based upon the feature of the solid and properties of interest. Those studies were carried out not only for academic understanding structural and mechanisms attributes of phase transitions but can also be of manufacturing great importance. Study of phase transitions in solid employs a broad selection of techniques including XRD, thermal and electrical conductivity methods.

[1a] Solid-State Physics Department, Physics Division, National Research Centre, Dokki, Giza, Egypt
[b] Electron Microscope and Thin Films Department, Physics Division, National Research Centre, Dokki, Giza, Egypt
[c] Nanoscience laboratory for environmental and biomedical applications (NLEBA), Physics Department, Faculty of Education, Ain Shams University, Roxy, Cairo, Egypt, *Corresponding author e-mail: amamansour@gmail.com

Solid electrolytes, or superionic conductors, of the type A_2BI_4 (A=Ag, Cu; B=Hg) are deemed as model subjects to review of phase changes into a high ionic conductivity condition. It is supposed that within the superionic phase passage, the iodide sublattice persists, whilst in the superionic phase A^+, B^{2+} and stoichiometric vacancies V_A^+, which are allocated arbitrarily in the crystalline lattice, identify the high conductivity of the superionic material [7,8]. These materials have recently become of industrial importance as recording media, particularly in the infrared region [7,8].

Silver mercury iodide Ag_2HgI_4 is a material with a face-centered cubic (f.c.c.) anion arrangement situated in tetragonal (β) phase at room temperature and cubic (α) phase at elevated heat conditions. Ag_2HgI_4 has an order-disorder transition at about 52°C. The structure of α-Ag_2HgI_4 is identical to that of the β-phase, with the exception that the iodine sublattice currently is an ideal f.c.c. arrangement and diffraction studies reveal that the cations were irregularly arranged over half of the tetrahedrally coordinated positions [9]. Crystallographically, α-Ag_2HgI_4 is bounded in the cubic space group $F\bar{4}3m$ with every cation location taking an average occupancy of ½ Ag and ¼ Hg^{-2} [8,9]. The primitive Wiegner-Seitz cell shows S_4 symmetry and the lattice parameters as a = 6.3 Å and c = 12.6 Å at room temperature[8,9].

In this study, structure, composition, and morphology of Ag_2HgI_4 were investigated by means of X-ray diffraction, EDX, and scanning electron microscope (SEM) respectively. Also, phase transformation was studied by differential thermal analysis (DTA) at 5, 10, 15, 20, 25, and 30 degrees/minute heating rates. Kinetics of the found thermal transitions was analyzed by Kissinger, Ozawa, and Augis-Bennett approaches respectively.

2. Experimental techniques

2.1. Materials preparation

The Ag_2HgI_4 powder was prepared by a solvothermal method using $AgNO_3$, KI, and HgI_2 as a starting material. Briefly, 25 mL of a 1M solution of $AgNO_3$ in deionized water and 40 mL of a 2M solution of KI dissolved in deionized water were mixed under stirring for 10 minutes. Then, 15 mL of a 1M solution of HgI_2 dissolved in hot ethanol is added to the mixture prepared in the previous step and mixed together at room temperature and stirred for 30 minutes. The resulted solution is transferred into 100 mL capacity Teflon-line stainless steel autoclave and kept at 200 °C for 8h. After this time period, the autoclave was cooled to room temperature and the formed yellow precipitates of Ag_2HgI_4 were separated by filtration. The product powder was washed repeatedly with water and ethanol several times until it becomes free of any such impurities. Finally, the Ag_2HgI_4 nanoparticles are dried at room temperature.

2.2. Characterization methods

The structural properties of Ag_2HgI_4 powder have been investigated by X-ray diffraction (XRD) using Philips X-ray diffractometer (Type X'Pert) with monochromatic CuKα radiation, operating at 40 kV and 25 mA. The surface morphology of the prepared films was studied using scanning electron microscope interfaced with Energy dispersive X-ray (EDX) (Quanta FeG250).
The thermal behavior was investigated by using differential thermal analysis instrument type (TA-60WS Thermal Analyzer Shimadzu). The DTA was carried out on approximately 10 mg quantities of powder samples, the measurements were carried out under a nitrogen atmosphere, the cell used from aluminum has flow rate = 20 (mL/min) and the accuracy of the heat flow is ±0.01mW. The samples were heated at different rates (5, 10, 15, 20, 25 and 30 ◦C/min), that remain constant for every heating process and their thermograms were recorded. The measurements were made under the same experimental conditions for all samples at each heating rate values.

3. Results and discussions

3.1. Structural, compositional and morphological results of Ag_2HgI_4 powder

The X-ray diffraction spectrum of the Ag_2HgI_4 powder is depicted in Fig. 1. The existence of sharp peaks in the diffractograms proves that the studied powder is polycrystalline in nature. In order to identify the various diffraction peaks, the experimental d-values of Ag_2HgI_4 powder were compared with those of the standard diffraction data file (JCPDS card No. 74-0168). The d-values are in good coincidence with those of the standard values without any extra planes that might reveal the creation of any secondary phases. Therefore, the studied powder is formed in a single phase with tetragonal structure and space group $1\bar{4}\,(82)$ as well as exhibits a dominant orientation along (112) diffraction. It is worth noting that the dominant diffraction differs from the one informed on the aforementioned JCPDS card. Such variances are probably resulting from the difference of growth mechanism arising from the difference of deposition operation [10].

The lattice constants of the powder (a, c) were estimated from the h k l plane using the below equation [11,12]:

$$\frac{1}{d^2} = \frac{h^2+k^2}{a^2} + \frac{l^2}{c^2} \quad (1)$$

The estimated lattice parameters are a = b = 0. 632 nm and c =1.264 nm, which are in good agreement with the JCPDS values and earlier reported values [13].
The grain sizes D and the strain function ε of Ag_2HgI_4 powder were analyzed by Williamson-Hall (W-H) according to the relation [14,15]:

$$\beta \cos\theta = \frac{k\lambda}{D} + 4\varepsilon \sin\theta \quad (2)$$

Where β is the full width at the half maximum, k is the shape factor ≈ 0.94 and λ is the wavelength of the incident X-rays (λ = 0.15406 nm). Fig. 2 shows Williamson-Hall plots for Ag_2HgI_4 powder. The data points were fitted to a straight line by the least-squares method, where the y-intercept gives the grain size and the slope is a measure of strain. The values of the grain size D and the strain ε of the powder are found to be 67 nm, $1.51x10^{-2}$, respectively.

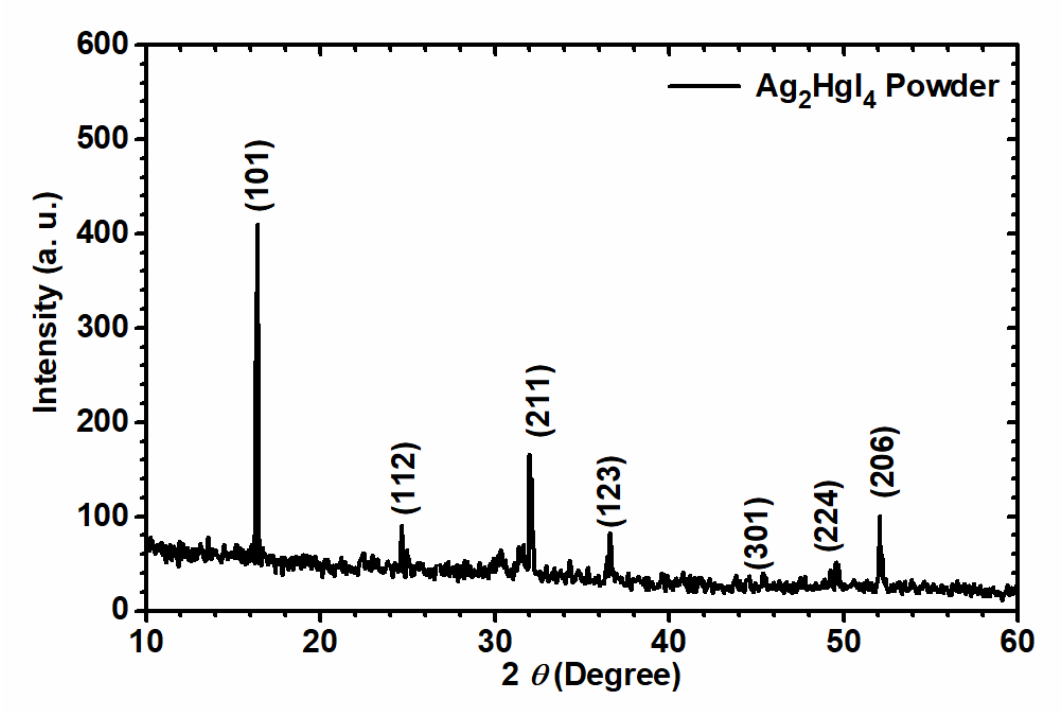

Fig. 1 X-ray diffraction pattern for Ag_2HgI_4 nano-powder.

Dislocations are an essential property that directly affects the electrical properties of the material because it is considered a type of defects and disorders in the lattice. The dislocation density δ was estimated by the next relation [16]:

$$\delta = \frac{1}{D^2} \tag{3}$$

The calculated value of dislocation was found to be 2.23 X 10^{10} lines/cm^2.

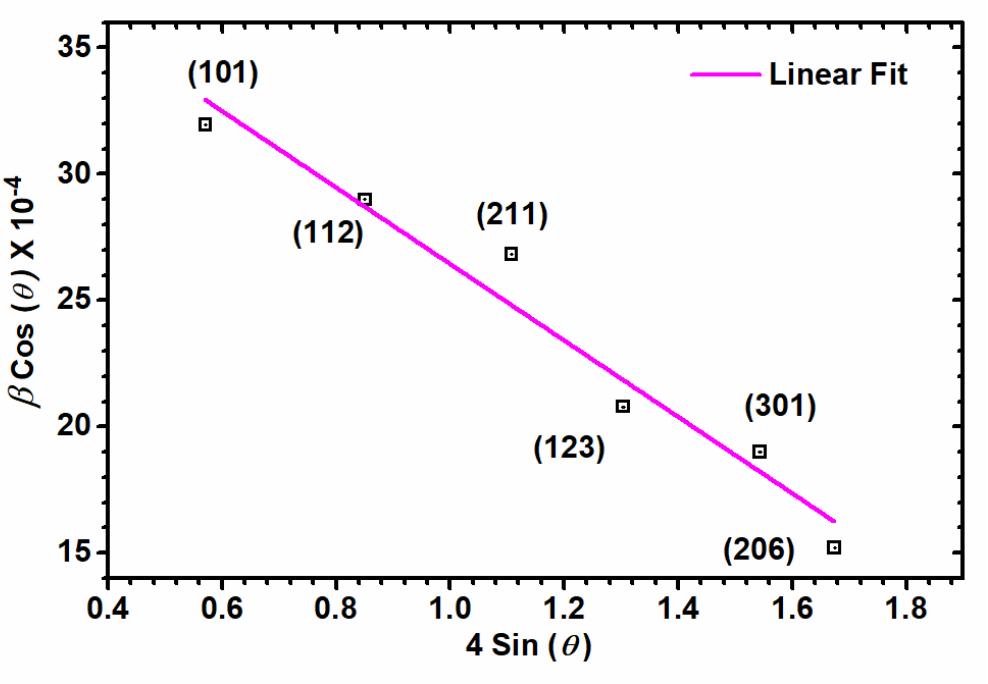

Fig. 2 Plot of 4sin(θ) versus βcos(θ) of Ag_2HgI_4 Nano-powder.

Fig. 3 shows the EDX spectrum of typical representative Ag_2HgI_4 powder prepared by the solvothermal method. The pattern confirms the presence of silver, mercury, and iodine.

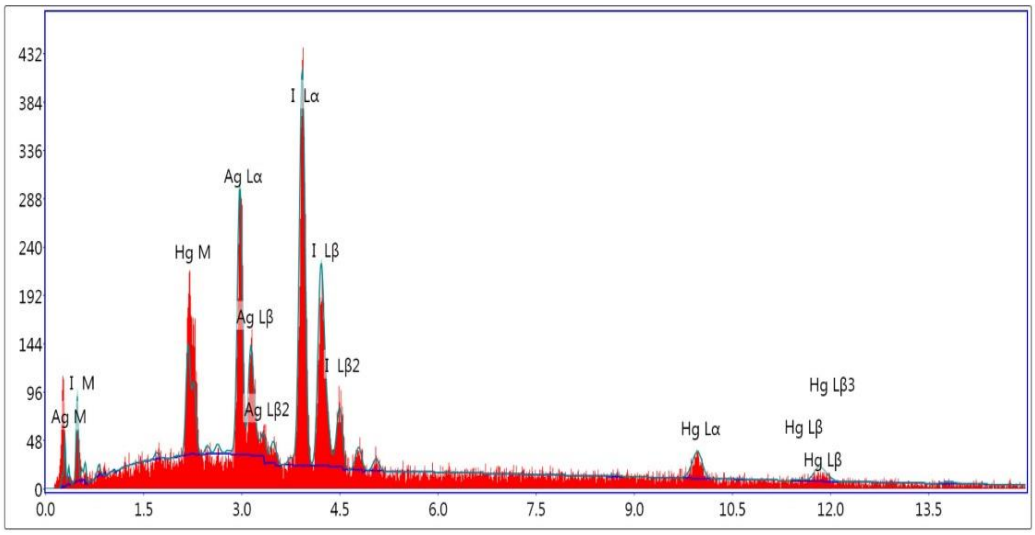

Fig. 3 The EDX of Ag_2HgI_4 Nano-powder

It has found that atomic percentages of these elements are Ag = 26.72, Hg = 15.83, I= 57.45, which correspond to 2:1:4 ratios. Therefore, the Ag_2HgI_4 powder is almost stoichiometric in composition.

Fig. 4 shows the surface micrograph of Ag_2HgI_4 powder prepared by the solvothermal method. Clearly, the surface Ag_2HgI_4 powder is homogenous and has a compact structure built from one type of microcrystals which are small, densed packed up and have a uniform distribution. The grains are distinct, tetragonal, and grain boundaries are distinguishable. It was found that the grain size varies from 64 to 95 nm and the average is 70 nm which is in a good agreement with that found by XRD method.

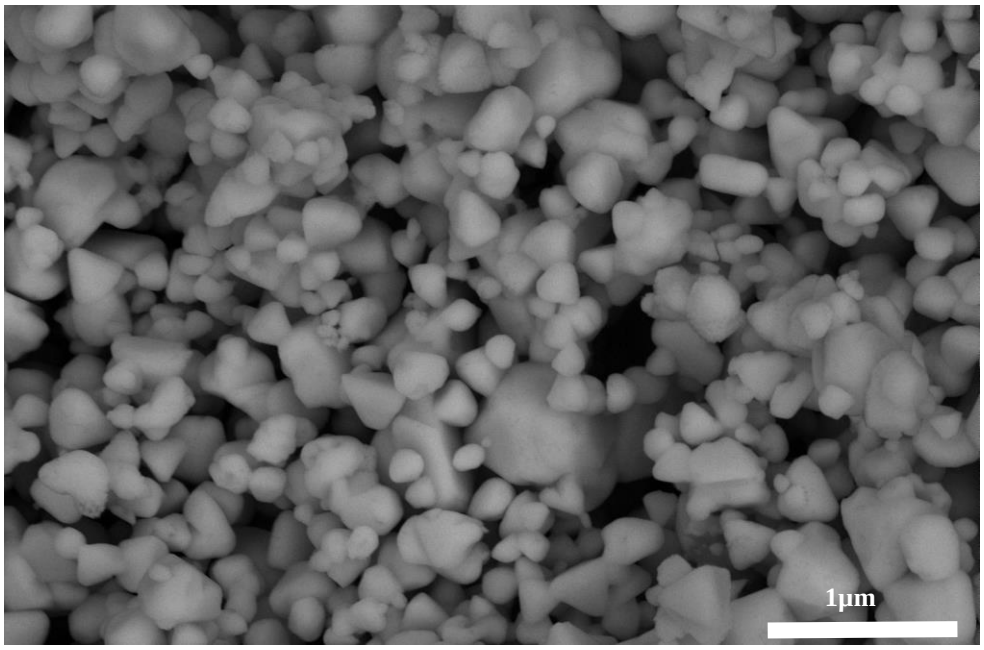

Fig. 4 The surface micrograph of Ag_2HgI_4 Nano-powder.

3.2. Calculations of E_1, E_2 and T_m for Ag_2HgI_4 according to different models

Thermal first-order change, just like melting step, is characterized by an interruption or discontinuity in both the volume and enthalpy behavior with heating at the transition point [17]. Second order changes are characterized by just a slope swapping and a deviation in the first derivative is located [18]. Accordingly, the glass transition temperature, Tg, ıs not a first-order type, where either volume or entropy shows no discontinuities with the temperature at a transition point. Even so, the first derivative of the physical quantity-temperature behavior displays a notable alter in the T_g position; therefore, it is often labeled as a second-order type [19–21].

Figures 5, 6, 7, 8, 9 and 10 show the phase transformations of the Ag_2HgI_4 sample at 5, 10, 15, 20, 25 and 30 ◦C/min heating rates respectively. For all heating rates, three characteristic phenomena are evident. All the DTA curves contained three endothermic peaks. The first change temperature point (T_1) in Ag_2HgI_4 is mentioned as a first order β→α broken, interrupted or discontinuous superionic passage and the other change at a second peak (T_2) could be outlined on the basis of cation disordered superionic state in Ag_2HgI_4 [22–24]. The third endothermic peak related to melting point (T_m) of the sample [23]. Additionally, it is noticed that the values of T_1, T_2 and T_m increase with increasing heating rate from 5 to 30 ◦C/min, for the composition under investigation as given in Table 1.

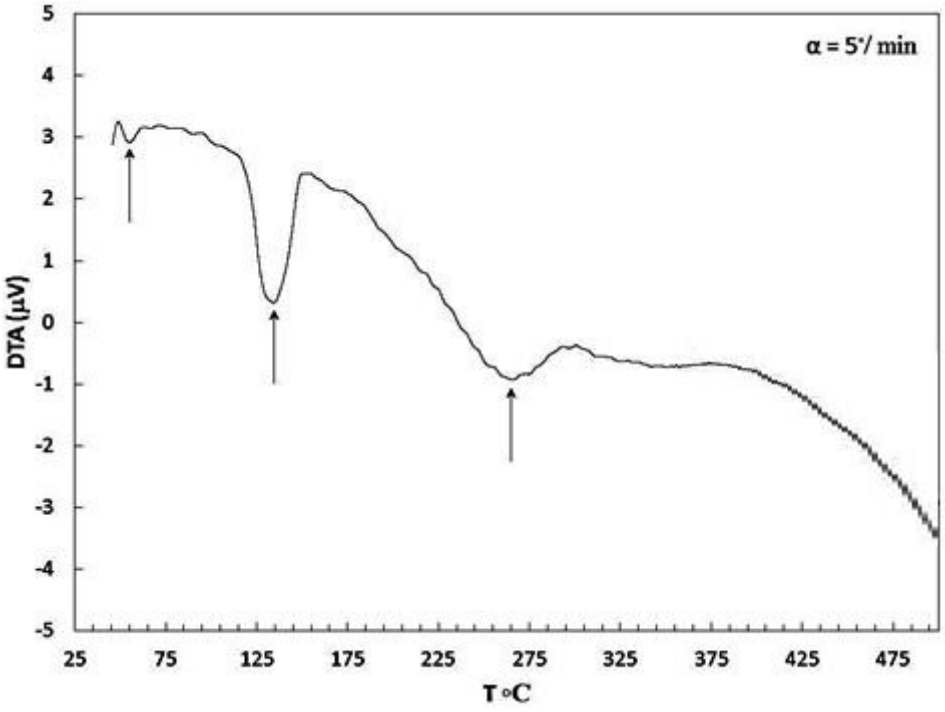

Fig. 5 DTA trace of Ag_2HgI_4 at 5°/min heating rate.

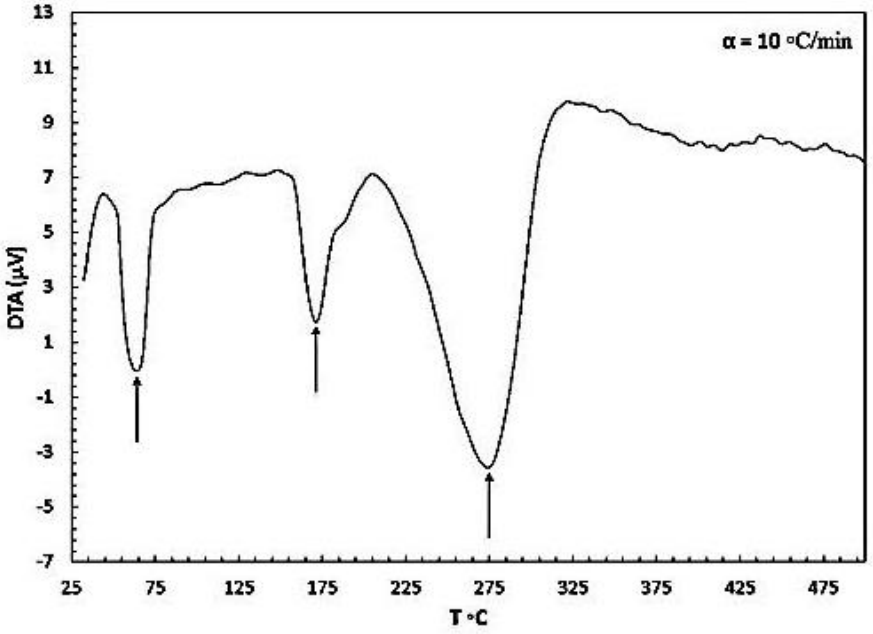

Fig. 6 DTA trace of Ag_2HgI_4 at 10°/min heating rate.

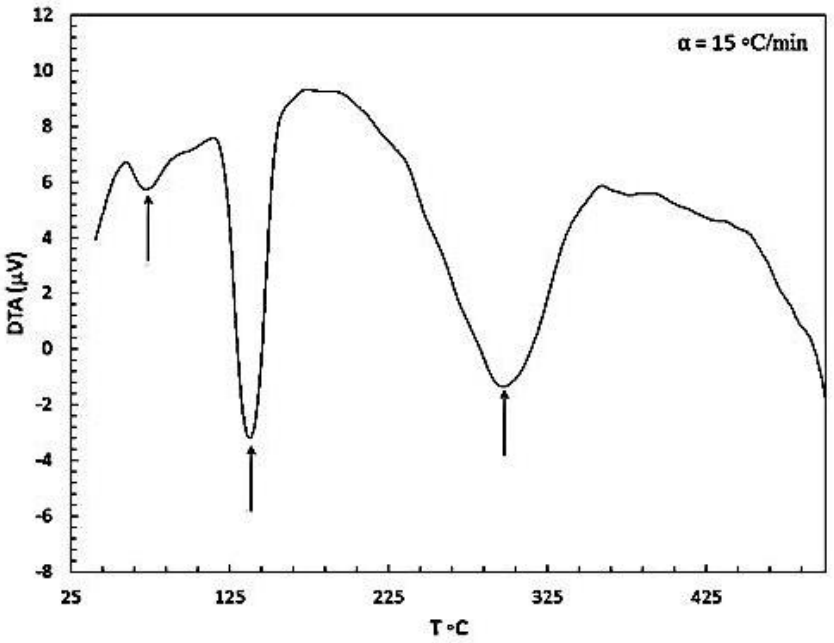

Fig. 7 DTA trace of Ag_2HgI_4 at 15°/min heating rate.

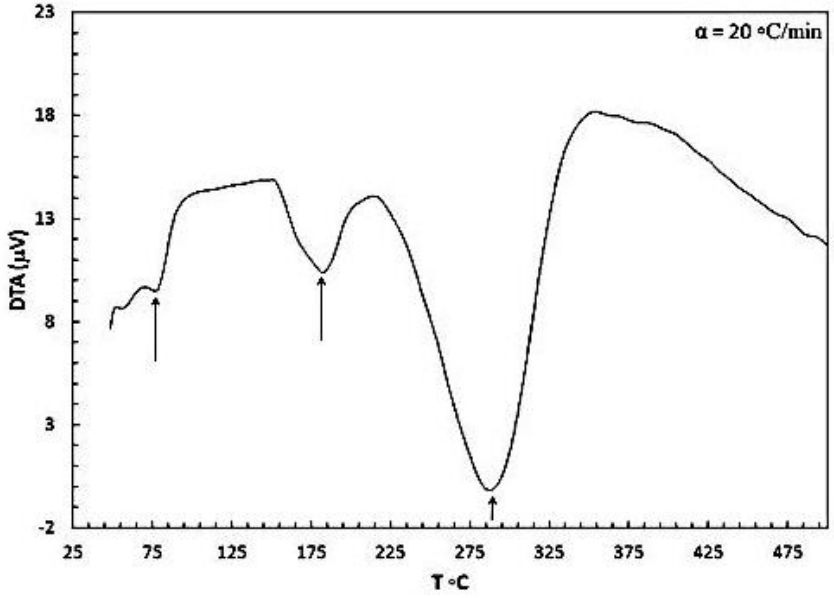

Fig. 8 DTA trace of Ag_2HgI_4 at 20°/min heating rate.

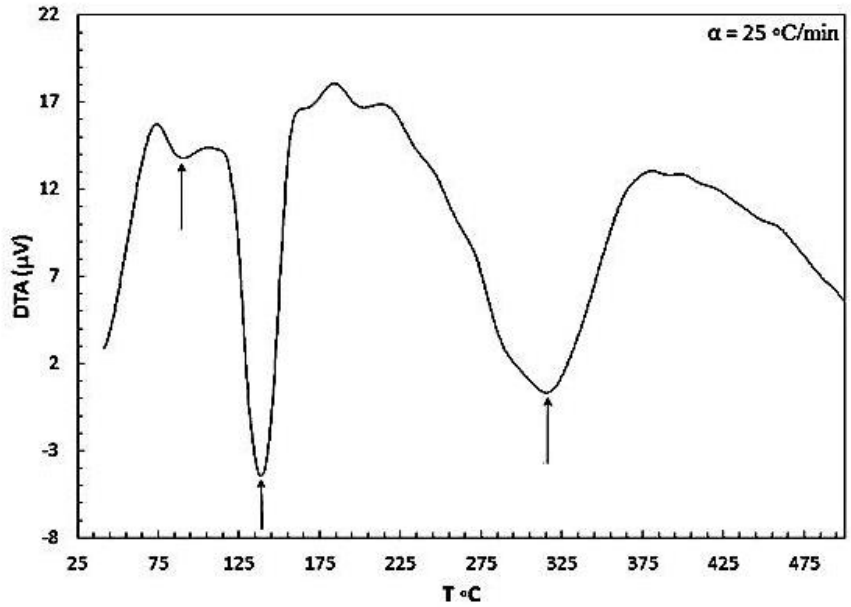

Fig. 9 DTA trace of Ag_2HgI_4 at 25°/min heating rate.

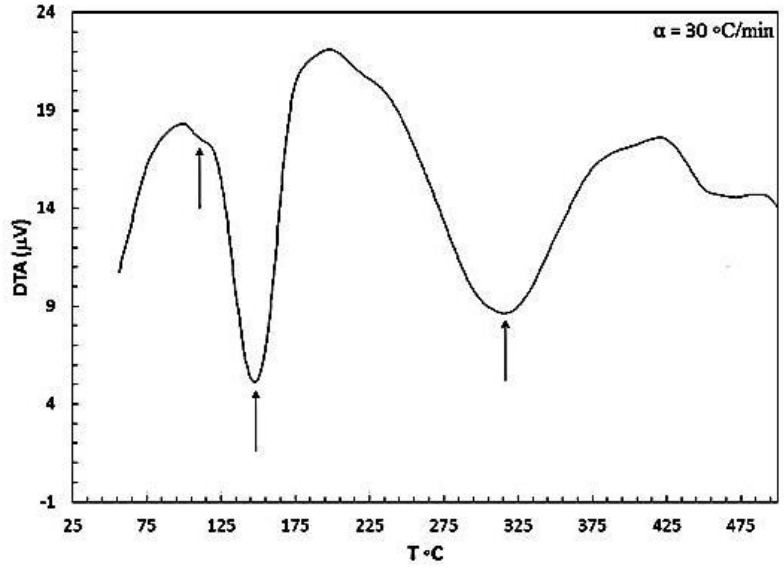

Fig. 10 DTA trace of Ag_2HgI_4 at 30°/min heating rate.

Table 1

Values of T_1, T_2 and T_m at different heating rates.

Heating rate α	T_1 (°C)	T_2 (°C)	T_m (°C)
5	54	131	261
10	59	168	271
15	67	135	287
20	74	181	291
25	86	136	313
30	102	146	316

This can be explained as follows, in DTA at the lower heating rate the sample temperature is very close to that shown by the instrument as heat is well transferred. When the rate increases, the sample cannot take up the heat so fast and get close to the instrument temperature, the change occurs later. Eventually, the increase in temperature is obtained. These amounts to sample showing a phase transition at a higher temperature.

Thermal analysis techniques, especially differential thermal analysis (DTA) were utilized successfully [25] in exploring phase transformations including nucleation, growing, continuing grain progress of pre-existing nuclei and for understanding the kinetics of crystallization of solids. Kinetic information on first order changes is frequently attained via this approach in both isothermal and non-isothermal process. The isothermal evaluation is somewhat more defined; typically it has been found that the non-isothermal technique, as well as many

features, including that experiments, can be executed rapidly. Besides that, various phase transitions take place very rapidly to be measured within isothermal variables due to transients caused by the experimental apparatus. For this reason, non- isothermal techniques are commonly used for reviewing the kinetics of phase transitions of solids.

A lot of researchers used the famous Kissinger model [26] or Ozawa model [27] directly to review the glassy state transition kinetics or crystallization process kinetics. Such ways, however, could not be utilized directly to the crystallization process, and thus, the considered activation energy (E_A) physical meaning is unknown since the crystallization is developed by the action of nucleation and growth stages and not by the reaction of n-th order. Otherwise, some authors have implemented the Johnson-Mehl-Avrami formula for the operation of non-isothermal type [28–32]. The higher is the activation energy the higher is the stability of the sample. As mentioned by Vallejos-Burgos, in this case, the value of E_a only reflects the sensitivity of the rate of the process towards temperature. However, the rate of the process is scaled by the preexponential factor which is equally important. So, the stability of the material is assessed by calculating some physically meaningful quantity such as reaction rate, isoconversional time, etc. [33–35].

The activation energies of E_1, E_2, and E_m for the transition phases of the investigated material can be determined to utilize unique models of Kissinger, Ozawa-Augis, and Bennett.

3.2.1. Kissinger approach

As stated by Kissinger model, the reaction rate optimum takes place with a rise in the temperature [26]. The alteration degree at the event peak of the DTA relation is a constant at several heating rates. This method is a model-free approach and it is not an iso-conversional one as it concerns constant activation energy in the rising of change. Even though it was formerly created for the crystallization events, it has become accessible and suitable in general manner [36–38]. Kissinger equation is expressed as[26,39]:

$$ln\left(\alpha/T_p^2\right) = ln(k_0 R/E_a) - \left(E_a/RT_p\right) \quad (4)$$

Where T_p represents the peak temperature and R is the gas constant.

Consequently, kinetic variables including activation energy (E_a) and preexponential factor (frequency factor) (k_0) can be acquired from a plot of $ln(\alpha/T_p^2)$ versus $1000/T_p$ for a series of experiments at different heating rates.

Figures 11, 12 and 13 show the plots of $ln(\alpha/T_p^2)$ versus $1000/T_p$ for the observed three transition peaks, i.e. at T_1, T_2 and T_m. The plots give liner relations. The values of E_1, E_2 and E_m, are obtained from the slopes of trend lines according to Kissinger and listed in Table 2.

3.2.2. The approach of Flynn-Wall-Ozawa (FWO)

The Kissinger-Akahira-Sunose (FWO) strategy is established on the below formula [40]:

$$\ln(\alpha) = ln\left(\frac{AE_a}{Rg(x)}\right) - 5.331 - 1.052\frac{E_a}{RT_p} \quad (5)$$

Thus, for a constant conversion, a plot of the natural logarithm of heating rates, $ln(\alpha)$ against $1000/T_p$ collected from thermal plots captured at distinct heating rates will be a straight line whose slope $(-1.052(E_a/RT))$ will calculate the activation energy.

Figures 11, 12 and 13 show the plots of $ln(\alpha)$ versus $1000/T_p$ for the observed three transition peaks, i.e. at T_1, T_2 and T_m. The plots give liner relations. The values of E_1, E_2 and E_m are obtained from the slopes of trend lines according to Flynn-Wall-Ozawa (FWO) and listed in Table 2.

3.2.3. Augis-Bennett Evaluation

The activation energy of the observed transition process, E_1, E_2, and T_m, may well be motivated by an evaluation methodology evolved by Augis and Bennett [41]. They employed the next formula:

$$\ln(\alpha/T_p) = (-E_p/RT_p) + lnk_0 \quad (6)$$

$\ln(\alpha/T_p)$ change with $1000/T_p$ yields a straight line. Its slope is used to obtain the value of activation energy of the transition process (E_1, E_2 and E_m).

Figures 11, 12 and 13 show the plots of $ln(\alpha/T_p)$ versus $1000/T_p$ for the observed three transition peaks, i.e. at T_1, T_2 and T_m. The plots give liner relations. The values of E_1, E_2 and E_m, are obtained from the slopes of the trend lines according to Flynn-Wall-Ozawa (FWO) and listed in Table 2.

Table 2

Values of E_1, E_2 and E_m (Kcal/mol.) for according to Kissinger, Ozawa, and Augis

Transition process / Method	E_1 Kcal/mol	E_2 Kcal/mol	E_m Kcal/mol
E_a according to Kissinger	1.844	2.396	13.882
E_a according to Ozawa	8.295	2.322	18.233
E_a according to Aguis	7.600	1.471	17.115
K_0 (S^{-1})	$2.7x10^3$	4.884	$1.2x10^5$

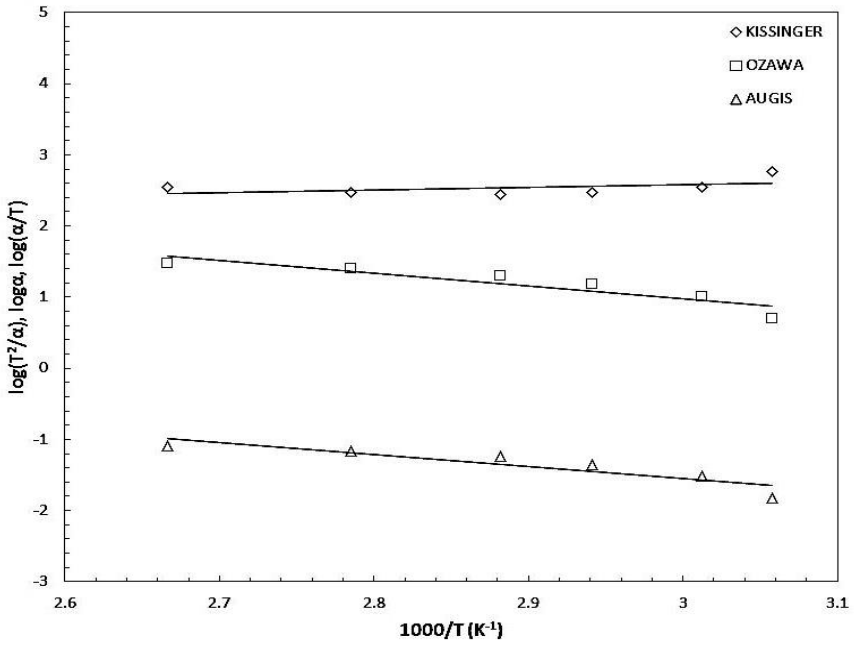

Fig. 11 Plots of $\log(T^2/\alpha)$, $\ln(\alpha)$, and $\log(\alpha/T)$ versus 1000/T for Ag_2HgI_4 according to Kissinger, Ozawa and Augis models respectively for 1st transition.

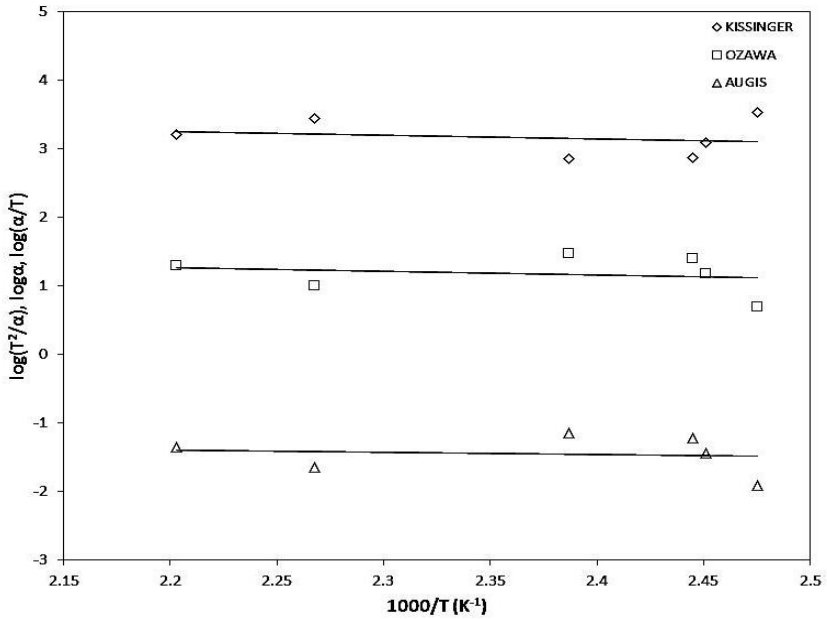

Fig. 12 Plots of $\log(T^2/\alpha)$, $\ln(\alpha)$, and $\log(\alpha/T)$ versus 1000/T for Ag_2HgI_4 according to Kissinger, Ozawa and Augis models respectively for 2nd transition.

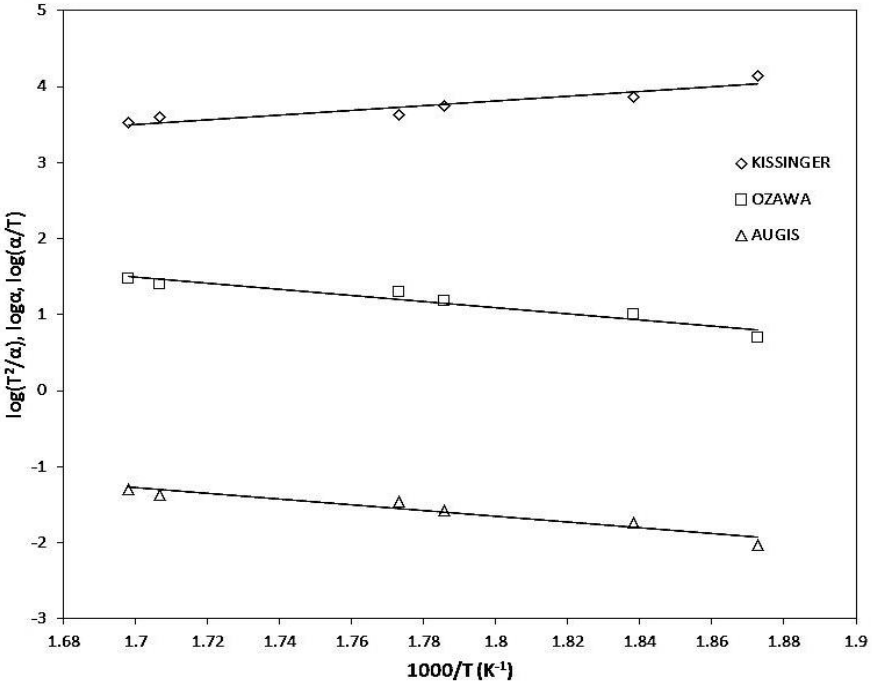

Fig. 13 Plots of $\log(T^2/\alpha)$, $\ln(\alpha)$, and $\log(\alpha/T)$ versus 1000/T for Ag_2HgI_4 according to Kissinger, Ozawa and Augis models respectively for 3rd transition.

4. Conclusions

The phase transition of Ag_2HgI_4 powder was studied by differential thermal analysis (DTA) at 5, 10, 15, 20, 25, and 30 degrees/minute heating rates. Non-isothermal apparent activation energies of observed transition process were calculated by Kissinger, Flynn-Wall-Ozawa and Augis-Bennett approach respectively. The kinetics of phase transformation of the Ag_2HgI_4 system was studied by using non-isothermal analysis method. Investigation of the heating rates dependence α = 5, 10, 15, 20, 25, and 30 degrees/minute on T_1, interrupted or discontinuous superionic passage, T_2, cation disordered superionic state in Ag_2HgI_4, and T_m, melting point were done by using DTA analysis. The difference in the resulted values of E_1, E_2, and E_m using different theoretical models may be attributed to the different approximation used in these models. The values of E_1, E_2, and E_m increases with increasing α. The activation energy is useful in understanding thermal relaxation phenomena in these phases' changes.

R E F E R E N C E S

[1] A. Ben-Naim, D. Casadei, Modern thermodynamics, World Scientific, New Jersey, 2017.
[2] M. Lumsden, M. Steinitz, E.J. McAlduff, Phase transitions involving vacancy ordering in two metal

mercuric iodides, Ag 2 HgI 4 and Cu 2 HgI 4, J. Appl. Phys. 77 (1995) 6039–6041. doi:10.1063/1.359189.

[3] M. PaiĆ, V. PaiĆ, Phases, phase transitions and excitons of the superionic conductor Cu 2 HgI 4 , from 4.2 K to 373 K, as revealed by the Kubelka-Munk spectral function, Phase Transitions. 56 (1996) 11–20. doi:10.1080/01411599608207835.

[4] Noorussaba, A. Ahmad, Phase transition in a [Ag2HgI4:0.2AgI] mixed composite system doped with KI, Russ. J. Electrochem. 49 (2013) 1065–1072. doi:10.1134/S1023193512080125.

[5] C. Julien, G.-A. Nazri, Solid State Batteries: Materials Design and Optimization, Springer US, Boston, MA, 1994. doi:10.1007/978-1-4615-2704-6.

[6] D.W. Readey, Kinetics in materials science and engineering, Taylor & Francis Group, Florida, 2017. https://www.worldcat.org/title/kinetics-in-materials-science-and-engineering/oclc/948748532&referer=brief_results (accessed November 13, 2017).

[7] A.M. Salem, Y.A. El-Gendy, G.B. Sakr, AC Conductivity and Dielectric Properties of Cu2HgI4, Chinese J. Phys. 47 (2009) 874–884.

[8] S. Hull, D.A. Keen, Structural characterization of further high temperature superionic phases of Ag 2 HgI 4 and Cu 2 HgI 4, J. Phys. Condens. Matter. 13 (2001) 5597–5610. doi:10.1088/0953-8984/13/24/305.

[9] S. Hull, D.A. Keen, Structural characterization of the *betatoalpha* superionic transition in Ag 2 HgI 4 and Cu 2 HgI 4, J. Phys. Condens. Matter. 12 (2000) 3751–3765. doi:10.1088/0953-8984/12/16/302.

[10] H.-L. Su, Y. Xie, Z.-P. Qiao, Y.-T. Qian, Formation of Cu2−xSe(en)2 in a solvothermal process and conversion to nanocrystalline Cu2−xSe, Mater. Res. Bull. 35 (2000) 1129–1135. doi:10.1016/S0025-5408(00)00305-6.

[11] A.E. Blagov, M. V. Dekapoltsev, M. V. Kovalchuk, V. V. Lider, Y. V. Pisarevsky, P.A. Prosekov, Lattice Parameter Local Determination for Trigonal, Hexagonal, and Tetragonal Crystal Systems Using Several Coplanar X-Ray Reflections, Crystallogr. Reports. 55 (2010) 1074–1078. doi:10.1134/S106377451006026X.

[12] A.A.M. Farag, F.S. Terra, G.M. Mahmoud, A.M. Mansour, Study of Gaussian distribution of inhomogeneous barrier height for n-InSb/p-GaAs heterojunction prepared by flash evaporation, J. Alloys Compd. 481 (2009) 427–433. doi:10.1016/j.jallcom.2009.03.004.

[13] J.W. Brightwell, C.N. Buckley, R.C. Hollyoak, B. Ray, Structural and phase equilibrium comparisons of Ag2HgI4 with Ag2CdI4 and Ag2ZnI4, J. Mater. Sci. Lett. 3 (1984) 443–446. doi:10.1007/BF00724388.

[14] G.. Williamson, W.. Hall, X-ray line broadening from filed aluminium and wolfram, Acta Metall. 1 (1953) 22–31. doi:10.1016/0001-6160(53)90006-6.

[15] M.Z. Butt, D. Ali, H. Farooq, F. Bashir, Structural, electrical, and mechanical characteristics of proton beam irradiated Al5086 alloy, Phys. B Condens. Matter. 456 (2015) 275–282. doi:10.1016/j.physb.2014.09.014.

[16] G.K. Williamson, R.E. Smallman, III. Dislocation densities in some annealed and cold-worked metals from measurements on the X-ray debye-scherrer spectrum, Philos. Mag. 1 (1956) 34–46. doi:10.1080/14786435608238074.

[17] P. Papon, J. Leblond, P.H.E. Meijer, The physics of phase transitions : concepts and applications, Springer-Verlag, Berlin, 2006. https://www.worldcat.org/title/physics-of-phase-transitions-concepts-and-applications/oclc/228160958&referer=brief_results (accessed April 13, 2017).

[18] B. Fultz, Phase transitions in materials, Cambridge University Press, New York, 2014. https://www.worldcat.org/title/phase-transitions-in-materials/oclc/891185196&referer=brief_results (accessed April 13, 2017).

[19] M.E. Brown, Introduction to Thermal Analysis: Techniques and Applications, Kluwer Academic Publishers, Dordrecht, 2001. doi:10.1017/CBO9781107415324.004.

[20] M.E. Brown, Handbook of thermal analysis and calorimetry. Volume 1, Principles and practice, Elsevier, 1998.

[21] E.M. El-Menyawy, I.T. Zedan, A.M. Mansour, H.H. Nawar, Thermal stability, AC electrical conductivity and dielectric properties of N-(5-{[antipyrinyl-hydrazono]-cyanomethyl}-[1,3,4]thiadiazol-2-yl)-benzamide, J. Alloys Compd. 611 (2014) 50–56. doi:10.1016/j.jallcom.2014.05.120.

[22] M. Hassan, M.S. Nawaz, Rafiuddin, Ionic conduction and effect of immobile cation substitution in

binary system $(AgI)_{4/5}-(PbI_2)_{1/5}$, Radiat. Eff. Defects Solids. 163 (2008) 885–891. doi:10.1080/10420150801900634.

[23] R.C. Agrawal, R. Kumar, Investigation on ionic transport properties and solid state battery applications of a new Ag^+ ion conducting glass system X(0.75AgI:0.25AgCl):(1-X)(Ag_2O:B_2O_3), J. Phys. D. Appl. Phys. 27 (1994) 2431–2437. doi:10.1088/0022-3727/27/11/027.

[24] T.A. Hameed, I.M.E. Radaf, G.B. Sakr, Synthesis and characterization of thermochromic Ag2HgI4 thin films, Appl. Phys. A Mater. Sci. Process. 124 (2018) 684. doi:10.1007/s00339-018-2107-2.

[25] D.K.S. Rathore, N.S. Saxena, Kinetics of Phase Transformations and Thermal Stability of Se58Ge42-xPbx (x = 15, 18 & 20) Glasses, New J. Glas. Ceram. 02 (2012) 23–33. doi:10.4236/njgc.2012.21005.

[26] H.E. Kissinger, Reaction Kinetics in Differential Thermal Analysis, Anal. Chem. 29 (1957) 1702–1706. doi:10.1021/ac60131a045.

[27] T. Ozawa, Thermal analysis — review and prospect, Thermochim. Acta. 355 (2000) 35–42. doi:http://dx.doi.org/10.1016/S0040-6031(00)00435-4.

[28] J. Colmenero, J.. Barandiaràn, Crystallization of Al23Te77 glasses, J. Non. Cryst. Solids. 30 (1979) 263–271. doi:10.1016/0022-3093(79)90165-0.

[29] A. Lucci, L. Battezzati, C. Antonione, G. Riontino, Influence of preannealing on crystallization kinetics of some metallic glasses, J. Non. Cryst. Solids. 44 (1981) 287–295. doi:10.1016/0022-3093(81)90031-4.

[30] D.W. Henderson, Thermal analysis of non-isothermal crystallization kinetics in glass forming liquids, J. Non. Cryst. Solids. 30 (1979) 301–315. doi:10.1016/0022-3093(79)90169-8.

[31] E.A. Marseglia, Kinetic theory of crystallization of amorphous materials, J. Non. Cryst. Solids. 41 (1980) 31–36. doi:10.1016/0022-3093(80)90188-X.

[32] K. Harnisch, R. Lanzenberger, Determination of the avrami exponent by non-isothermal analyses, J. Non. Cryst. Solids. 53 (1982) 235–245. doi:10.1016/0022-3093(82)90083-7.

[33] P. Šimon, Induction periods : Theory and applications, J. Therm. Anal. Calorim. 84 (2006) 263–270. doi:10.1007/s10973-005-7204-z.

[34] P. Šimon, Z. Cibulková, P. Thomas, Accelerated thermooxidative ageing tests and their extrapolation to lower temperatures, J. Therm. Anal. Calorim. 80 (2005) 381–385. doi:10.1007/s10973-005-0664-z.

[35] P. Šimon, Material stability predictions applying a new non-Arrhenian temperature function, J. Therm. Anal. Calorim. 97 (2009) 391–396. doi:10.1007/s10973-008-9627-5.

[36] M.A. El-Shahawy, Phase transformations of some poly(vinyl alcohol)-NiCl2 composites, Polym. Int. 52 (2003) 1919–1924. doi:10.1002/pi.1266.

[37] S. Mahadevan, A. Giridhar, A.K. Singh, Calorimetric measurements on as-sb-se glasses, J. Non. Cryst. Solids. 88 (1986) 11–34. doi:10.1016/S0022-3093(86)80084-9.

[38] M.. Wakkad, E.K. Shokr, S.. Mohamed, Optical and calorimetric studies of Ge–Sb–Se glasses, J. Non. Cryst. Solids. 265 (2000) 157–166. doi:10.1016/S0022-3093(99)00882-0.

[39] H. Ou, M. Sahli, T. Barriere, J.-C. Gelin, Determination of the activation energy of silicone rubbers using different kinetic analysis methods, MATEC Web Conf. (NUMIFORM 2016 12th Int. Conf. Numer. Methods Ind. Form. Process. Vol. 80 (2016) 16007. doi:10.1051/matecconf/20168016007.

[40] M. Heydari, M. Rahman, R. Gupta, Kinetic Study and Thermal Decomposition Behavior of Lignite Coal, Int. J. Chem. Eng. 2015 (2015) 1–9. doi:10.1155/2015/481739.

[41] J.A. Augis, J.E. Bennett, Calculation of the Avrami parameters for heterogeneous solid state reactions using a modification of the Kissinger method, J. Therm. Anal. 13 (1978) 283–292. doi:10.1007/BF01912301.